Hard and Protective Coatings

Mater. Res. Soc. Symp. Proc. Vol. 843 © 2005 Materials Research Society T1.2

Investigations of the effect of $(Cr_{1-x},Al_x)N$ coatings' micro Structure on Impact Toughness

K. Bobzin, E. Lugscheider, O. Knotek, M. Maes *

Material Science Institute, RWTH Aachen University, Augustinerbach 4-22,D-52056 Aachen, Germany

Abstract

Originated from the tooling industry, PVD (Physical Vapor Deposition) coating development focused on increasing the wear resistance. Nowadays, a steadily increasing market is evolving by coating machine parts. The requirements that have to be met due to the needs of this new market segment focus on tribological behavior. This means, that the focus of wear resistance is shifted towards properties like coefficient of friction, wetting behavior and the response of coatings towards dynamic loads. For many tribological applications, coatings are exposed to severe alternating loads, which are usually left out in common test methods. The approach of common coating test methods are based on the static behavior of deposited coatings. The impact tester is a testing device with a novel approach to dynamic load behavior of both bulk and coated materials. In this paper, the effect of the coatings' microstructure and Young's modulus on the impact toughness was investigated. A change in microstructure was provoked by changing deposition parameters like aluminum content. In a second stage these coatings were then tested with respect to their response to high alternating loads. For this purpose both load and number of impacts were varied.

Key words: CrAlN, impact testing, tribology

* M.Maes
Email address: maes@msiww.rwth-aachen.de (K. Bobzin, E. Lugscheider, O. Knotek, M. Maes).
URL: http:/www.rwth-aachen.de/ww (K. Bobzin, E. Lugscheider, O. Knotek, M. Maes).

1 Introduction

Physical Vapor Deposition (PVD) or Plasma Enhanced Chemical Vapor Deposition (PECVD) carbon based coatings are usually related to machine parts. Chromium based coatings are mostly not considered for this tribological application, since the dry friction coefficient is overshadowed by those of carbon based coatings. However, preliminary investigations[1] show, when lubricated, the friction torque in machine parts (for instance: cylindrical roller bearings) is equal to that of a low friction carbon based coating Graded Zirconium carbide (ZrC_g).

The advantages of chromium based coatings are manifold. Although Cr_xN exceeds the hardness of a hardened steel, it cannot match the hardness of TiN or TiC [2]. Its toughness is remarkable, yet difficult to quantify. Low surface energy of the immediately formed Chromium Oxides Cr_2O_3, when exposed to oxygen, can offer good protection against adhesive wear and corrosion. The formation of protective, passivating Cr_2O_3 coatings [3,4] also leads to an improved oxidation resistance ($< 800°C$), in comparison to TiN or TiC coatings ($< 550°C$). For this reason Cr_xN coatings are used amongst others for cutting of non-ferrous heavy metals and in plastic processing [5]. Other points of interest for tribological applications are the non depending friction coefficient against steel when exposed to air's humidity. Also the higher temperature stability than carbon based coatings is of interest. The compressive residual stress within these coatings can help to prevent thermal or mechanical crack initiation [6,7]. This is particularly interesting since most tribological applications deal with high alternating loads. Former impact testings have proven Cr_xN coatings to be more resistant against impact loading and were able to achieve a much higher service lifetime [9,10]. These arguments have left us to believe, that chromium based coatings show an extraordinary potential as a tribological coating. They can offer a perfect alternative, where carbon based coatings fail to perform.

The system $(Cr_{1-x},Al_x)N$ is a novel generation of chromium based coatings and extensively investigated by [11,12,7,13] at deposition temperatures of ($> 400°C$). By adding Aluminum the Young's modulus is altered and a composite coating generated. Also the addition of aluminum effected the structure of the synthesized coatings, although it is not suggested, that this is aluminium content related. Aim of this paper was to observe the dynamic load behavior of the differently synthesized coatings.

2 Experimental Details

Since coating development of machine parts is focus of this paper, steel (100Cr6) and carbide inserts were used for deposition. All samples were mirror polished and ultrasonically cleaned in alkaline solutions of different concentrations, rinsed with deionised water and finally dried. The 100Cr6 samples were subjected to a hardening and annealing process resulting in a final hardness of 60 Rockwell C. The samples were hardened at 860 °C for 1h and tempered for 2h at 180 °C. After cleaning, the samples are immediately batched in a pre conditioned deposition chamber and all three stages (Heating, Etching and Deposition) were carried out in this same chamber. Pre conditioning of the deposition chamber comprises baking out the vacuum chamber in order to get rid of entrapped water within the chamber walls.

The coating equipment was a CemeCon CC800/9 equipped with four Targets of either Aluminum and/or Chromium see Fig.1. The first two stages of the process, heating (T_{Max}=160 °C, 1h) and ion etching (1h) ensure a degassing and a full removal of surface oxides, which both strongly effects coating adhesion. The gas flow during deposition was controlled for both argon and nitrogen with a fixed ratio of Ar:N_2 resp. 300 sccm to 60 sccm resulting in a chamber pressure of 580 mPa. To avoid annealing of the temperature sensitive substrates the sum of power rates for all cathodes never exceeded 8kW during the entire deposition process. To generate coatings of different aluminium content, cathode arrangement and local cathode power was varied between 1 and 3kW see Table 1. However the sum was kept constant at 8kW at all times.

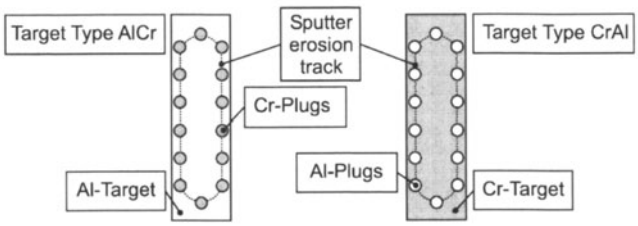

Fig. 1. Target design

Table 1
Experimental data on coating deposition

Batch	Position CrAl	Power	Position AlCr	Power
2054.CrAlN	1,2,3,4	4x2 kW	-	-
2070.CrAlN	1,3	2x1 kW	2,4	2x3 kW
2090.CrAlN	-	-	1,2,3,4	4x2 kW

The experimental values are given in ref. [14].

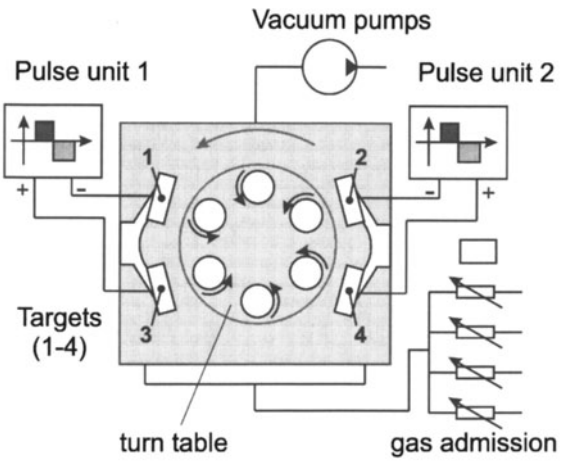

Fig. 2. Experimental setup

After deposition, the coating properties were determined with respect to coating thickness, adhesion [15], hardness and impact toughness. Nanoindentation (Equipment: MTS Systems Nanoindentation XP) was performed with a Berkovic indenter .The indenter penetrated the coated surface perpendicular at a constant load of 10 mN. Calculations of the Young's modulus are based on Oliver and Phar's equations [16,17] and Poisson ratio was kept constant at $\nu = 0.25$. Additionally both elastic and plastic deformation of the coating was calculated by numeric integration from the load/displacement curves Fig. 3. The plastic share is represented by the area under the release curve. The elastic share represented by the area enclosed by load and release curve. The calculated average values are listed in Table 2.

The 100Cr6 ($E = 210\ GPa$) flat ($r \to \infty$) samples were impacted in a test rig (Discription[8]) similar to [9] by carbide ($E = 630\ GPa$ [18]) balls Ø $5mm$ in diameter, at constant loads of 500, 600 and 700N with a frequency of $50Hz$. This load represents an equivalent of a maximum Hertzian contact pressure of respectively -7600, $-8000\ and\ -8500\ N/mm^2$.

$$\sigma_{Z,\,Max} = \sigma_0 = -\frac{1}{\pi} \cdot \sqrt[3]{\frac{1.5 \cdot F \cdot E^2}{r^2 \cdot (1-\nu^2)^2}} \tag{1}$$

$$\frac{1}{r} = \frac{1}{r_1} + \frac{1}{r_2} \tag{2}$$

$$E = 2 \cdot \frac{E_1 \cdot E_2}{E_1 + E_2} \tag{3}$$

Table 2
Deposition parameters and coating analysis.

Process ID	2054.CrAlN	2070.*CrAlN*	2090.*CrAlN*
$(Cr_{1-x},Al_x)N$	$x = 0.23$	$x = 0.48$	$x = 0.66$
$T_{R,\ Max}$ [°C]	120	190	120
Deposition time t_B [s]	4800	4800	8400
Deposition rate $\partial s/\partial$ t [μ m/h]	2.7	0.9	1.7
Coating thickness s_D [μ m]	3.6	1.2	3.9
Hardness Rockwell C	59 HRC	60 HRC	60 HRC
Coating hardness [GPa]	13.1	22.0	19.8
Young's modulus [GPa]	305	445	283
$W_{plastic}$[mN·nm]	541.5	389.2	421.8
$W_{elastic}$[mN·nm]	278.9	282.1	342.0
Ratio $W_{elastic}/W_{plastic}$	0.52	0.72	0.81
Adhesive strength HF [15]	HF 1	HF 1	HF 1
Critical Scratch Load L_C [N]	>90	20	70

The experimental values are given in ref. [14].

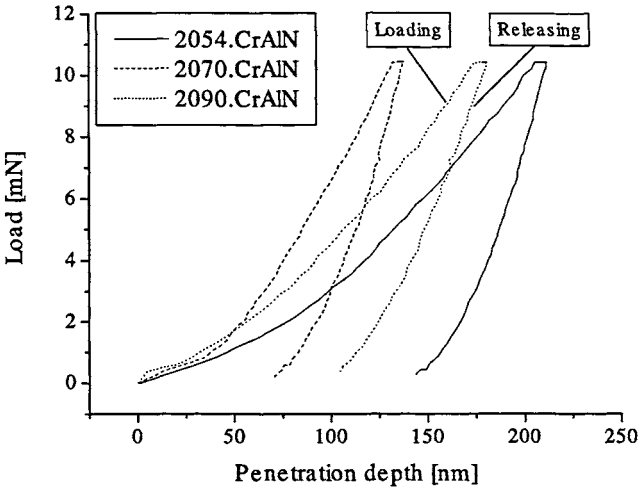

Fig. 3. Load/displacement curves CrAlN

3 Results

The results of mechanical testing are listed in Table 2. The coatings' microstructure is shown in Fig. 4. For both high and low aluminum contents (x=0.23 and x=0.66) a columnar growth of the coatings is observed. At an

aluminum content of x=0.48 this columnar growth disappears almost entirely, resulting in finer grained coating structure. This coating also exhibits highest hardness, Young's modulus and deposition temperature. Additionally a widening of the columns towards the surface is observed for the coating with lowest aluminum content (x=0.23). In contrast the coating with highest aluminum content (x=0.66) shows a more even, and smaller column width.

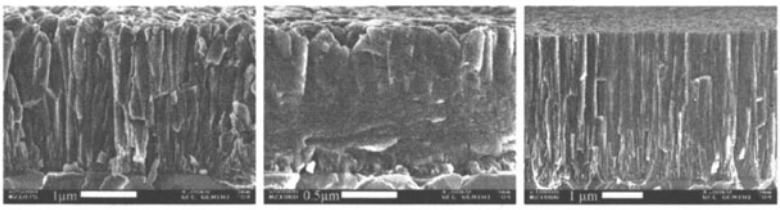

Fig. 4. SEM Fracture image 2054.CrAlN, 2070.CrAlN, 2090.CrAlN

The synthesized structures show a remarkable different behavior in impact testing. Fig. 5 reveals how the SEM images were evaluated. The right image is "intact" while the left is labelled as "failure" in case minute delamination is observed. In Fig. 6 results of all SEM investigations are sorted and visualized.

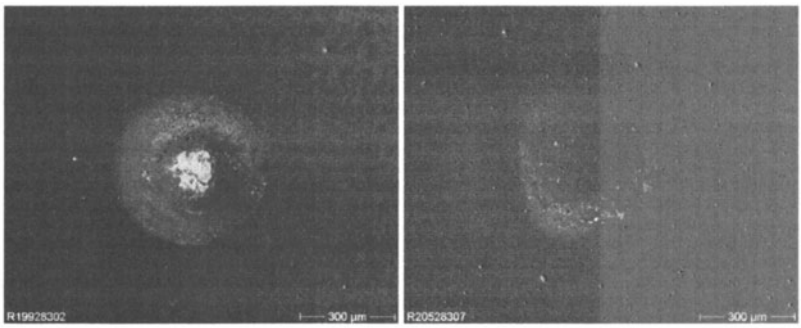

Fig. 5. SEM image 2054.CrAlN, 2090.CrAlN. Load: 600N, Impacts: 10^6

Most coatings eventually show small delaminations within the impact crater, similar to the left image Fig. 5, when either load or number of impacts is increased. Fig. 7 reveals a different behavior. The image reveals crack initiation at the border of the impact crater, whilst the center area of the impact is completely delaminated.

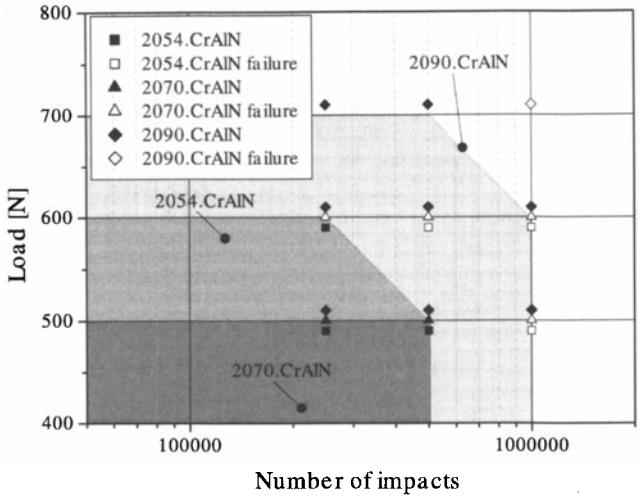

Fig. 6. Results impact testing of 2054.CrAlN, 2070.CrAlN, 2090.CrAlN

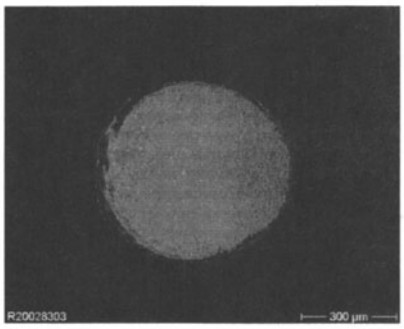

Fig. 7. SEM image 2070.CrAlN. Load: 600N, Impacts: 10^6

4 Discussion

The results show, that although all deposition parameters were kept constant a remarkable change in structure is observed for the coating with an aluminum content of x=0.48. This observation can be explained by the degree of target poisoning[19]. This is a phenomenon, which is observed when a surplus of reactive gas is present during sputtering. Consequently, during sputtering a reactive layer is formed at the targets' surface. The reactive heat will be dissipated at the cathodes. In case of reactive deposition heat gener-

ated is represented by the free Gibb's enthalpy ΔG_f° (see Table 3). Since the gas phase is unable to dissipate this heat, reaction will therefore only occur at surfaces, where heat can be dissipated. In the event of a poisoned target, the heat is eventually dissipated by the cooling circuit of the coating plant and does not add heat to the reactor. Whereas reactive deposition in the non poisoned mode leads to an increase in temperature since the substrate table is thermally isolated. The change in coating structure can be explained considering Thorton's deposition model [20]. The assumption is, that due to the reactive heat adatom mobility is increased, leading to a more dense isotropic structure. In Thornton's model these zones are marked by Zone I and Zone T. For coating 2070.CrAlN (x=0.48) a shift from ZoneI $\rightarrow$ Zone T is assumed resulting in a more fine, more dense istropic structure. By our means for all other aluminium contents a similar structure could be obtained by nitrogen flow adjustment(increase for x<0.48 and a decrease for x>0.48).

Table 3
Free Gibb's enthalpy ΔG_f°

Formula	Reaction	EntahlpyΔH°	ΔG_f°(773K)
CrN	$CrN \Leftrightarrow Cr + \frac{1}{2}N_2$	118-123[kJ/mol]	-61.6[kJ/mol]
AlN	$AlN \Leftrightarrow Al + \frac{1}{2}N_2$	289-318[kJ/mol]	-219.2[kJ/mol]

The experimental values are given in ref. [21].

With respect to impact resistance, columnar coating structures perform surprisingly well. Best performance is achieved by a fine grained columnar coating with a high aluminum content and a Young's modulus closest to the supporting substrate 100Cr6. The coating with an aluminum content of x=0.48 exhibits the worst impact resistance. It is likely to assume, that a lack of support caused by a decrease in hardness of the substrate is responsible for the low impact resistance. However no annealing effects (see Table 2) are observed and therefore no change in substrate hardness can be made responsible for a lack of support. Consequently, it is most likely, that either the columnar structure, the Young's modulus or a combination of both is responsible for the high impact toughness. Impact toughness is defined by the capability of the composite material to absorb or store impact energy without adding permanent damage to the material. In case of the columnar structure the energy induced by the impact is absorbed by friction between columns, plastic deformation or stored in elastic deformation. The columnar coating contains small intergranular spaces allowing the material to expand while being compressed. The induced tension is passed on to the substrate, without inducing tensile stresses parallel to the coating. In contrast, impact load applied to a fine granular structure will induce immediate tensile stresses within the coating causing rupture, flaking, break out etc.

The Young's modulus measured by nanoindentation is inevitably structure depending. Since the berkovich indenter penetrates the surface perpendicular and therefore in longitudinal axis of the column. Nanoindenter results between